Quasi-Solid-State Electrolyte Using an In Situ Click Reaction for Safety-Enhanced Lithium-Ion Batteries

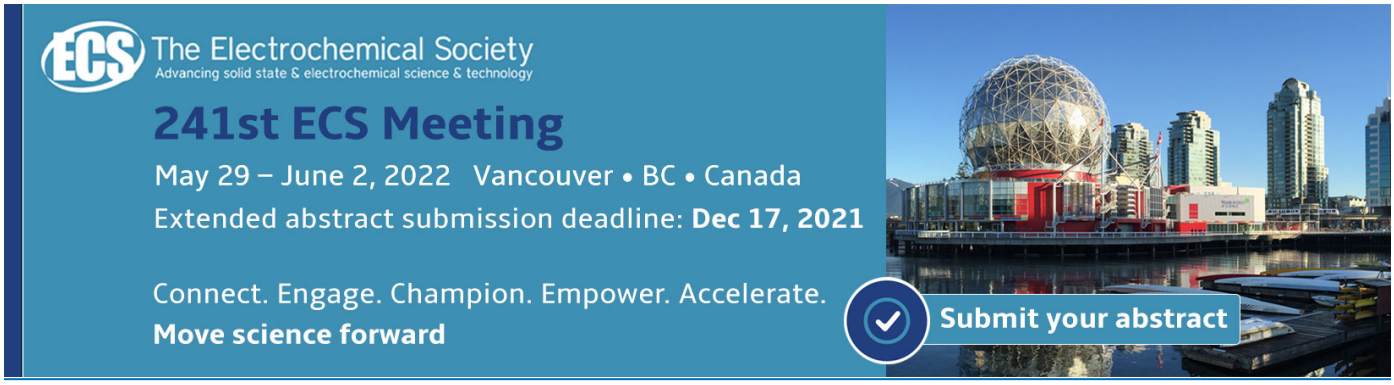

Journal of The Electrochemical Society, 2021 **168** 100538
1945-7111/2021/168(10)/100538/7/$40.00 © 2021 The Electrochemical Society ("ECS"). Published on behalf of ECS by IOP Publishing Limited

Quasi-Solid-State Electrolyte Using an In Situ Click Reaction for Safety-Enhanced Lithium-Ion Batteries

Bora Jeong,[=] Da-Ae Lim,[=] Hye-Min Kim, Jeong-Yun Kim, and Dong-Won Kim[z]

Department of Chemical Engineering, Hanyang University, Seoul 04763, Korea

Lithium-ion batteries with high energy density have been used widely as electrochemical energy storage devices to power mobile electronics, electric vehicles and large-sized energy storage systems. However, there are still safety concerns related to the highly flammable liquid electrolytes. As a highly safe electrolyte, we synthesized a three-dimensional quasi-solid-state electrolyte with high ionic conductivity of 2.1×10^{-3} S cm^{-1} using an in situ click reaction. Perfluoroether diacrylate with high oxidative stability was synthesized and used in in situ click reaction along with pentaerylythritol tetrakis(3-mercaptoptopionate) as the cross-linking agents. The lithium-ion cell composed of a graphite anode, a quasi-solid-state electrolyte and a $LiNi_{0.6}Co_{0.2}Mn_{0.2}O_2$ cathode was assembled, and its cycling characteristics and thermal stability were investigated. Our results reveal that the quasi-solid-state lithium-ion battery exhibits good capacity retention and superior thermal safety to conventional liquid electrolyte-based cells.
 [DOI: 10.1149/1945-7111/ac30ae]

Manuscript submitted August 20, 2021; revised manuscript received October 11, 2021. Published October 27, 2021.

Supplementary material for this article is available online

Lithium-ion batteries (LIBs) with high energy density and long cycle life are used widely in mobile electronics, electric vehicles and large-scale energy storage systems.[1–7] Unfortunately, current LIBs have safety issues such as fires and explosions under abnormal conditions due to the high flammability of liquid electrolyte and its leakage. For this reason, liquid electrolytes are not safe for use in high-energy density LIBs.[8,9] As an alternative, solid-state electrolytes can enhance the battery safety, because they are non-flammable and do not leak from the cell.[10–18] However, solid-state electrolytes have low ionic conductivity and high interfacial resistance due to their poor interfacial contact with electrodes during cycling. Quasi-solid-state electrolytes (QSEs) contain minimum amounts of organic solvents and exhibit combined advantages of liquid and solid-state electrolytes.[19–24] In QSEs, the polymer network encapsulates the flammable organic solvents, preventing their leakage and mitigating undesirable side reactions with electrodes. QSEs exhibit high ionic conductivity and good interfacial electrode contact due to small amounts of plasticizing organic solvent. Accordingly, many QSE systems have been developed to achieve both good electrochemical performance and improved battery safety.

In this work, we synthesized highly conductive QSEs with high oxidative stability using a click reaction. Click reaction has been known to reach a high degree of cross-linking in a short curing time under mild reaction conditions to form a durable chemical gel.[25–28] Perfluoroether diacrylate (PFE-Ac) with high oxidative stability was synthesized and used in the in situ click reaction with pentaerylythritol tetrakis(3-mercaptoptopionate) as the cross-linking agent. The optimized QSE was applied to the graphite/$LiNi_{0.6}Co_{0.2}Mn_{0.2}O_2$ cell. Its cycle performance and thermal stability were investigated, and compared with those of cell using liquid electrolyte.

Experimental Methods

Materials.—1H,1H,8H,8H-Perfluoro-3,6-dioxaoctan-1,8-diol (PFE-OH) was purchased from Exfluor Research Co. Tetrahydrofuran (THF, anhydrous) and acryloyl chloride (AC) were supplied by TCI Co. Ltd 4 Å molecular sieves were immersed in pentaerylythritol tetrakis(3-mercaptoptopionate) (PETMP, Sigma Aldrich) and methyl chloroform (99%, Sigma Aldrich) to remove residual moisture. Tert-butyl peroxypivalate (t-BPP) was purchased from Arkema and used as a click reaction initiator. Triethylamine (TEA, anhydrous), dimethyl carbonate (DMC, anhydrous), N-methyl-2-pyrrolidone (NMP, anhydrous) and bis(trifluoromethane) sulfonimide lithium (LiTFSI) were supplied by Sigma-Aldrich. LiTFSI was used after drying in a vacuum at 100 °C for 12 h. A polyethylene (PE) separator with a 9 μm thickness was supplied by SK Innovation and dried in a vacuum oven at 80 °C overnight before use. A battery-grade liquid electrolyte with 1.15 M $LiPF_6$ salt dissolved in a non-aqueous mixed solvent of ethylene carbonate (EC)/diethyl carbonate (DEC)/ethyl methyl carbonate (EMC) (3/2/5 by volume) solvent with 2 wt% vinylene carbonate (VC) was supplied by Dongwha Electrolyte Co. Ltd.

Synthesis of PFE-Ac.—PFE-OH (0.034 mol) and TEA (0.071 mol) were dissolved in THF (100 ml) at 0 °C under argon flow. Then, AC (0.071 mol) dissolved in THF (100 ml) was added to the solution using a syringe pump. After vigorous stirring for 48 h at 25 °C, the solution was filtered to remove precipitates and THF solvent was evaporated using a rotary evaporator at 50 °C. The residues were purified by column chromatography with methyl chloroform, yielding a colorless PFE-Ac.

Lithium-ion cell assembly.—The anode was composed of artificial graphite (91 wt%), poly(vinylidene fluoride) (PVdF) (8 wt%) and super-P carbon (1 wt%) on copper current collector. The cathode was $LiNi_{0.6}Co_{0.2}Mn_{0.2}O_2$, super-P carbon and PVdF (94:3:3 by weight) coated on aluminum current collector. Both anode and cathode were dried overnight at 80 °C in a vacuum oven. The active material mass loadings for the anode and cathode were 9.80 and 17.65 mg cm^{-2}, respectively. A CR2032-type coin cell was assembled by stacking a PE separator between the $LiNi_{0.6}Co_{0.2}Mn_{0.2}O_2$ cathode and graphite anode. To prepare a precursor solution for a quasi-solid-state electrolyte, PFE-Ac, PETMP and LiTFSI were dissolved in anhydrous DMC. t-BPP was added to the precursor solution as a click reaction initiator and stirred for 5 min. The precursor solution was injected into the cell and stored at 70 °C for 2 h to drive the in situ click reaction.

Characterization and measurements.—The ionic conductivity of the liquid electrolyte was obtained with a Cond 3210 conductivity meter (WTW GmbH) at 25 °C. In case of QSE, it was measured using an impedance analyzer (Zahner Electrik IM6) in the 10 Hz to 100 kHz frequency range with a 50 mV amplitude. Linear sweep voltammetry (LSV) was performed to evaluate the electrochemical stability of the electrolyte at 1 mV s^{-1} and 25 °C. ^{1}H NMR spectra were obtained for acetone d_6 solvent using a VNMRS 600 MHz spectrometer (Agilent Technologies). Attenuated Total Reflection-Fourier Transform Infrared (ATR-FTIR) spectroscopy was conducted using a Nicolet iS50 spectrometer. The cycling test of

[=]These authors contributed equally to this work.
[z]E-mail: dongwonkim@hanyang.ac.kr

lithium-ion cell was carried out using a battery tester (WBCS 3000 model, WonA Tech). Alternating current (AC) impedance spectra of the lithium-ion cells were obtained using an impedance analyzer over a frequency range from 1 mHz to 100 kHz before and after cycling. The morphologies of the electrodes were investigated with field-emission scanning electron microscopy (FE-SEM, JEOL JSM-6330F). To investigate the electrode thermal stability, electrodes (lithiated Li_xC anode and delithiated $Li_{1-x}Ni_{0.6}Co_{0.2}Mn_{0.2}O_2$ cathode) containing electrolyte (liquid electrolyte or QSE) were scraped from the current collector in the charged cell and crimp-sealed into a Tzero hermetic pan in an argon-filled glove box. Their thermal behavior was investigated by differential scanning calorimetry (DSC250, TA instrument) over a temperature range from 0 to 350 °C at a heating rate of 5 °C min^{-1}.

Results and Discussion

Perfluoroether diacrylate (PFE-Ac) was synthesized by substitution reaction using acryloyl chloride and perfluoroether diol (PFE-OH), as presented in Fig. S1 (available online at stacks.iop.org/JES/168/100538/mmedia). Its chemical structure was confirmed by FT-IR and ^{1}H NMR spectra. As depicted in Fig. 1a, the broad peak at 3300 cm^{-1}, corresponding to the stretching of -OH group in PFE-OH, was not observed in the product (PFE-Ac). Instead, two peaks were observed at 1744 and 1636 cm^{-1} in the PFE-Ac, which correspond to C=O and C=C stretching peaks of diacrylate, respectively. Figure 1b presents the ^{1}H NMR spectra of PFE–OH and PFE-Ac. The -OH peak at 2.3 ppm disappeared after the –OH group was substituted by acrylate, and the characteristic proton peaks of acrylate in PFE-Ac were observed in the range of 6.0 to 6.5 ppm. In addition, the $–CH_2–$ peak was slightly shifted downfield after acrylate substitution. These results revealed that the –OH groups in PFE–OH were substituted successfully with acrylate containing reactive double bond, which allowed PFE-Ac to be used as a cross-linking agent in the thiol-ene click reaction.

Figure 2a shows the schematic for the preparation of a precursor solution containing PETMP and PFE-Ac, and the synthesis of cross-linked QSE through a click reaction at 70 °C for 2 h. Table I summarizes the composition of the precursor solutions (QSE-S3, QSE-S4 and QSE-S5). The DMC content was fixed at 40 wt% in the precursor solution. The obtained QSEs were flexible rubbery films with no solvent exudation, indicating quasi-solid state. By increasing cross-linking agents (PETMP and PFE-Ac) in the precursor solution, the physical properties of the QSEs became more robust. The click reaction between PFE-Ac and PETMP was confirmed by analyzing FT-IR spectra of PFE-Ac, PETMP and QSE. As shown in Fig. 2b, both the C=C double bond peak of PFE-Ac at 1636 cm^{-1} and the S-H thiol peak of PETMP at 2572 cm^{-1} were absent in the QSE-S5 after the click reaction. This result suggests that alkene (C=C double) and thiol (S-H) react to form the three-dimensional polymer network through the thiol-ene click reaction, as schematically presented in Fig. 2a.

Figure 3a shows the ionic conductivities of the QSEs as a function of temperature. As expected, the ionic conductivities increased with temperature due to the increase of ionic mobility. Among three QSE types, QSE-S5 exhibited the highest ionic conductivities over all temperature ranges. This can be attributed to the increase in both number of free ions and their mobility, since QSE-S5 has a high salt concentration and a low degree of cross-linking. QSE-S5 exhibited a high ionic conductivity of 2.1×10^{-3} S cm^{-1} at 25 °C. Linear sweep voltammograms of QSEs with different composition are depicted in Fig. 3b. The anodic stability of QSE increased with increasing PFE-Ac and PETMP contents. This can be attributed to the high oxidative stability of perfluoroether used as a cross-linking agent.[29] The fluorine atoms with high electronegativity in PFE-Ac can disperse the electron

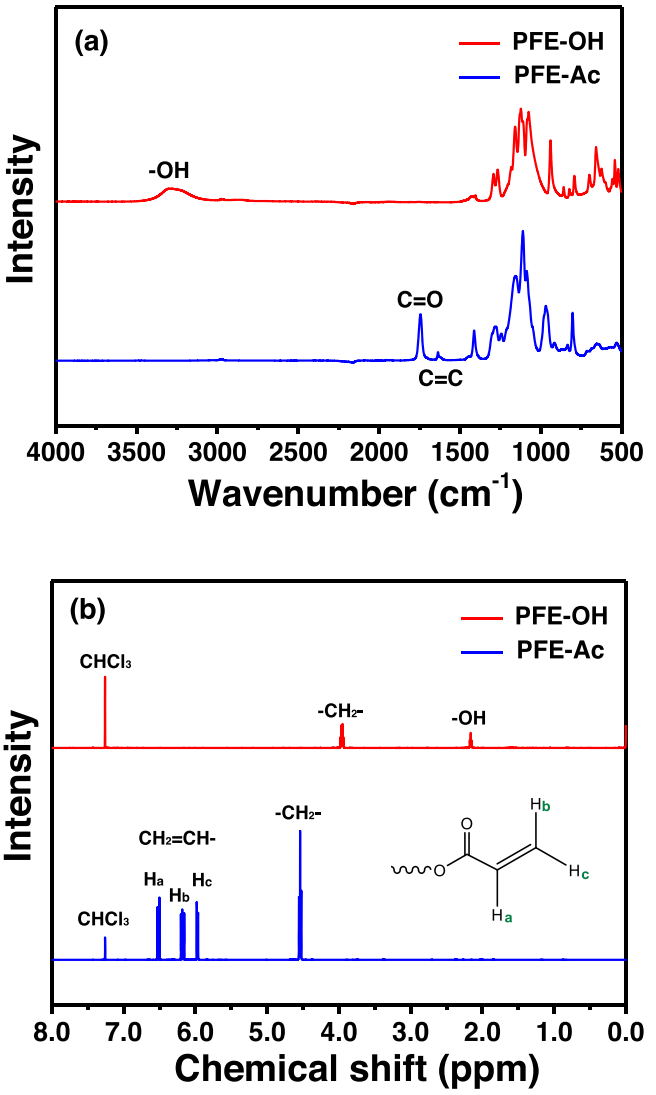

Figure 1. (a) FT-IR spectra of PFE-OH and PFE-Ac. (b) ^{1}H NMR spectra of PFE-OH and PFE-Ac in $CDCl_3$.

density as electron-withdrawing groups, improving oxidative stability. In addition, the liquid electrolyte (LiTFSI in DMC) is trapped well in the three-dimensional polymer network synthesized from PFE-Ac and PETMP, which mitigates oxidative decomposition of the liquid electrolyte. This was confirmed by comparing the linear sweep voltammograms of QSE-5 and liquid electrolyte with the same composition except cross-linking agent (Fig. S2). The anodic decomposition voltage was higher in QSE-5 than the liquid electrolyte, indicating that cross-linking using PFE-Ac and PETMP enhances the anodic stability of electrolyte at high-voltage regions. Based on the results discussed above, we chose QSE-S5 for the electrolyte system when assembling lithium-ion cells due to its highest ionic conductivity among the three QSEs and acceptable electrochemical stability for safe operation of the lithium-ion cell.

We assembled a lithium-ion cell (graphite/$LiNi_{0.6}Co_{0.2}Mn_{0.2}O_2$) using the optimized gel precursor solution (QSE-S5). As an additive for forming the solid electrolyte interphase (SEI) layer, 2 wt% VC was added to the precursor solution. The assembled cell was cured thermally at 70 °C for 2 h to drive the in situ click reaction. Before the cycling test, we conducted two pre-conditioning cycles at a 0.05 C rate to form a stable SEI layer on the graphite anode. After

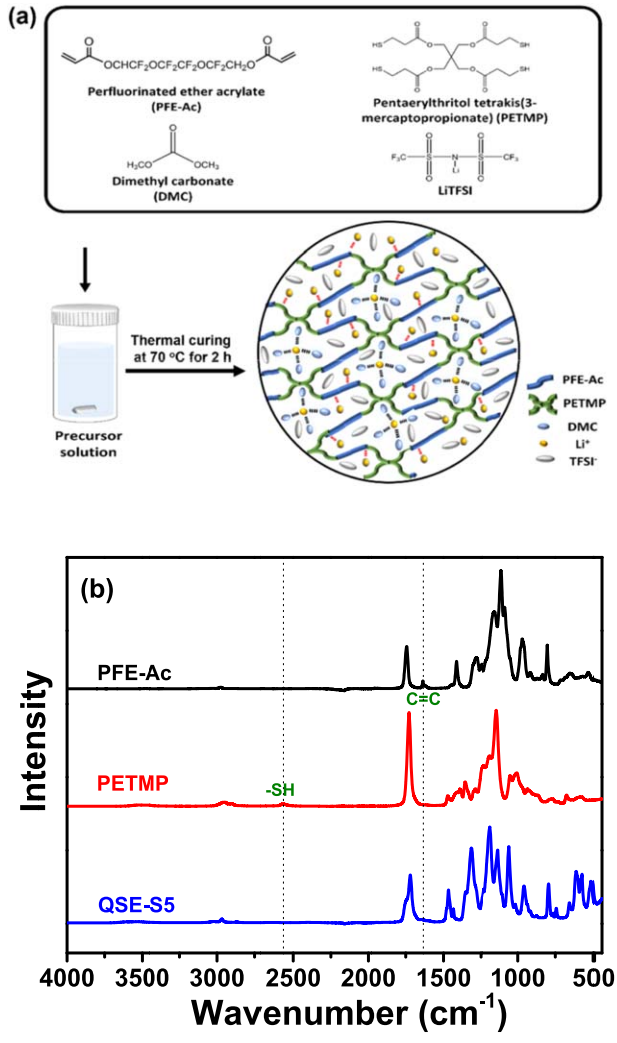

Figure 2. (a) Schematic illustration of cross-linked quasi-solid-state electrolyte (QSE) synthesis. (b) FT-IR spectra of starting materials (PFE-Ac, PETMP) and final product (QSE-S5) after cross-linking reaction.

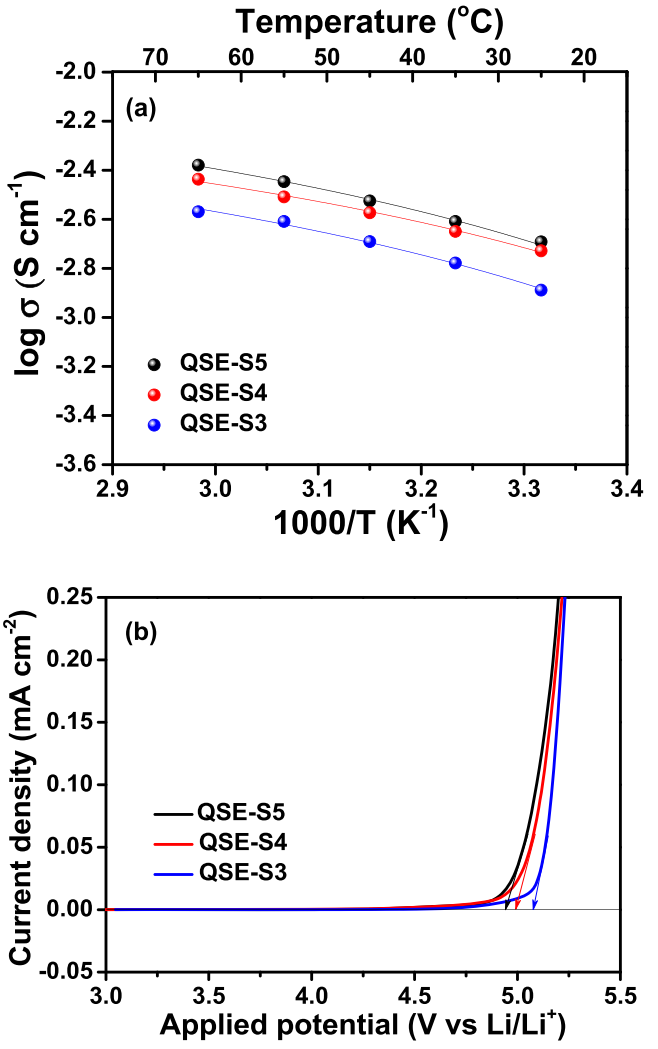

Figure 3. (a) Ionic conductivities and (b) linear sweep voltammograms of QSEs with different gel precursor compositions.

that, the cell was cycled within the cut-off voltages (3.0–4.2 V) at 0.2 C rate. The lithium-ion cell with a conventional liquid electrolyte (1.15 M $LiPF_6$-EC/DEC/EMC with 2 wt% VC) was also tested at the same test conditions. Figure 4a depicts the charge and discharge voltage profiles of the cell with QSE-S5 after two pre-conditioning cycles. The cell showed an initial discharge capacity of 142.9 mAh g^{-1} based on the active cathode material. The capacity was steadily increased until the 20th cycle, which is related to the activation of quasi-solid-state electrolyte during initial cycles. The activation process in the quasi-solid-state lithium-ion cell should be as short as possible to avoid waste of energy consumption and production time.[30,31] The gel precursor solution in this work was highly viscous (~18 cP) due to the low content of organic solvent and the active mass loadings in the electrodes were relatively high. Thus, it took a lot of time for the viscous precursor to fully penetrate into the thick electrodes (anode and cathode), which resulted in a long activation. The cell exhibited stable cycling behavior without noticeable capacity fading during cycling. Figure 4b compares the cycling performance of the cells with liquid electrolyte and QSE. Although the cell with QSE initially delivered a lower discharge capacity, its capacity retention was superior to that of the cell employing liquid electrolyte. Moreover, the quasi-solid-state cell exhibited stable

Table I. Composition of precursor solution for synthesizing quasi-solid-state electrolytes.

Precursor	PFE-Ac (wt%)	PETMP (wt%)	LiTFSI (wt%)	DMC (wt%)
QSE-S5	6.2	3.8	50	40
QSE-S4	12.4	7.6	40	40
QSE-S3	18.6	11.4	30	40

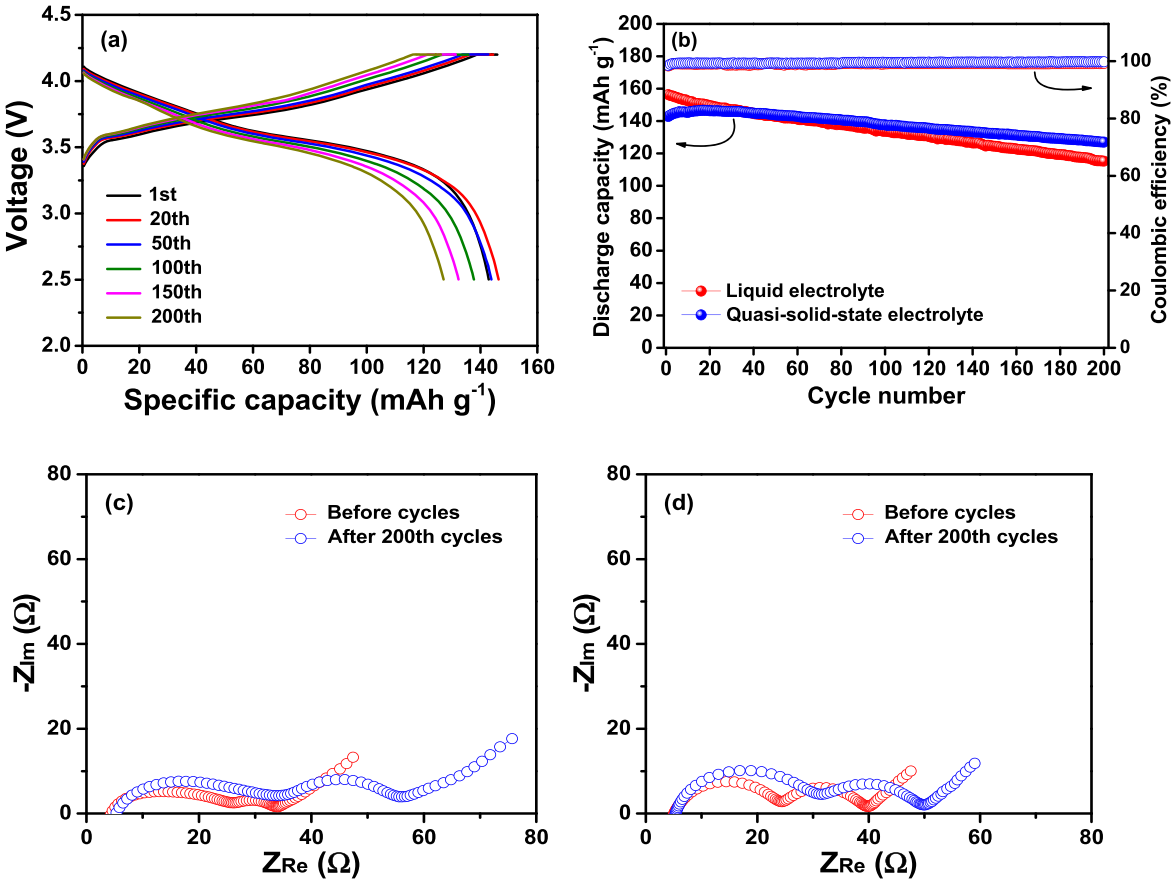

Figure 4. (a) Charge and discharge curves of the lithium-ion cells assembled with QSE-S5 at 25 °C. (b) Discharge capacities and coulomb efficiencies of the lithium-ion cells with liquid electrolyte and quasi-solid-state electrolyte (QSE-S5) as a function of cycle number at 25 °C. AC impedance spectra of the cells with (c) liquid electrolyte and (d) quasi-solid-state electrolyte before and after cycles.

Coulombic efficiencies higher than 99.4% throughout cycling after initial activation. AC impedance spectra of the cells were obtained before and after cycling. As shown in Figs. 4c and 4d, the cells exhibited two overlapped semicircles, which can be attributed Li^+ ion migration in the surface film formed on the electrode (R_f, high-to-medium frequency range) and charge transfer reaction at electrolyte-electrode interface (R_{ct}, medium-to-low frequency range), respectively. Although the quasi-solid-state cell showed slightly higher interfacial resistances than liquid electrolyte-based cell before cycling, the increase of interfacial resistances (R_f and R_{ct}) after 200 cycles was relatively small as compared to the cell with liquid electrolyte. During the in situ click reaction, the chemical cross-linking of the precursor formed strong interfacial contact between the electrolyte and electrodes, resulting in stable cycling of the QSE-based cell. Moreover, the encapsulation of organic solvent in the QSE can suppress its deleterious reactions on the electrodes during the repeated cycling and allow stable charge transfer reaction at electrolyte-electrode interface. From these results, we conclude that using a cross-linked QSE synthesized by in situ click reaction improves the cycling stability of lithium-ion cells.

We investigated the morphologies of electrodes before and after cycling. As presented in Figs. 5a and 5d, the pristine $LiNi_{0.6}Co_{0.2}Mn_{0.2}O_2$ cathode before cycling shows the porous structure, which provides enough space for the precursor solution or liquid electrolyte to deeply penetrate into the electrode during the cell assembly. The $LiNi_{0.6}Co_{0.2}Mn_{0.2}O_2$ particles cycled in liquid electrolyte (Figs. 5b and 5e) exhibited intergranular cracked morphologies due to the mechanical stress applied to the particles during the repeated cycling.[32–36] These cracks lead to more side reactions with the liquid electrolyte and isolation of the active materials, resulting in gradual deterioration of cell performance with cycling.[37] In contrast, the $LiNi_{0.6}Co_{0.2}Mn_{0.2}O_2$ cathode cycled in QSE (Figs. 5c and 5f) maintained its initial structure without significant mechanical damage, and the ionic conduction pathway was well connected through QSE, allowing stable cycle performance. The graphite anode showed no noticeable difference between the electrodes cycled in the two electrolytes, as shown in Fig. S3. The graphite particles cycled in QSE are covered with quasi-solid-state electrolyte, which has been formed during in situ cross-linking reaction of precursor solution.

The rate capability of the cells was evaluated at different current rates. Figure 6a shows the discharge curves of the lithium-ion cells assembled with QSE at C rates from 0.1 C to 2.0 C. Both cell voltage and discharge capacity decreased as C rate increased due to the increase of overpotential and voltage drop at high current rates. Figure 6b presents the discharge capacities of the cells assembled with different electrolytes at every five cycles at different C rates. The cell with QSE delivered lower discharge capacities due to the lower ionic conductivity of QSE. Ionic conductivity of liquid electrolyte was 8.4×10^{-3} S cm^{-1} at 25 °C, which is 4.2 times higher than that of QSE. However, the QSE-based cell recovered a high discharge capacity at 0.1 C rate after repeating high-rate cycles, indicating a more stable cycling behavior than liquid electrolyte-based cell.

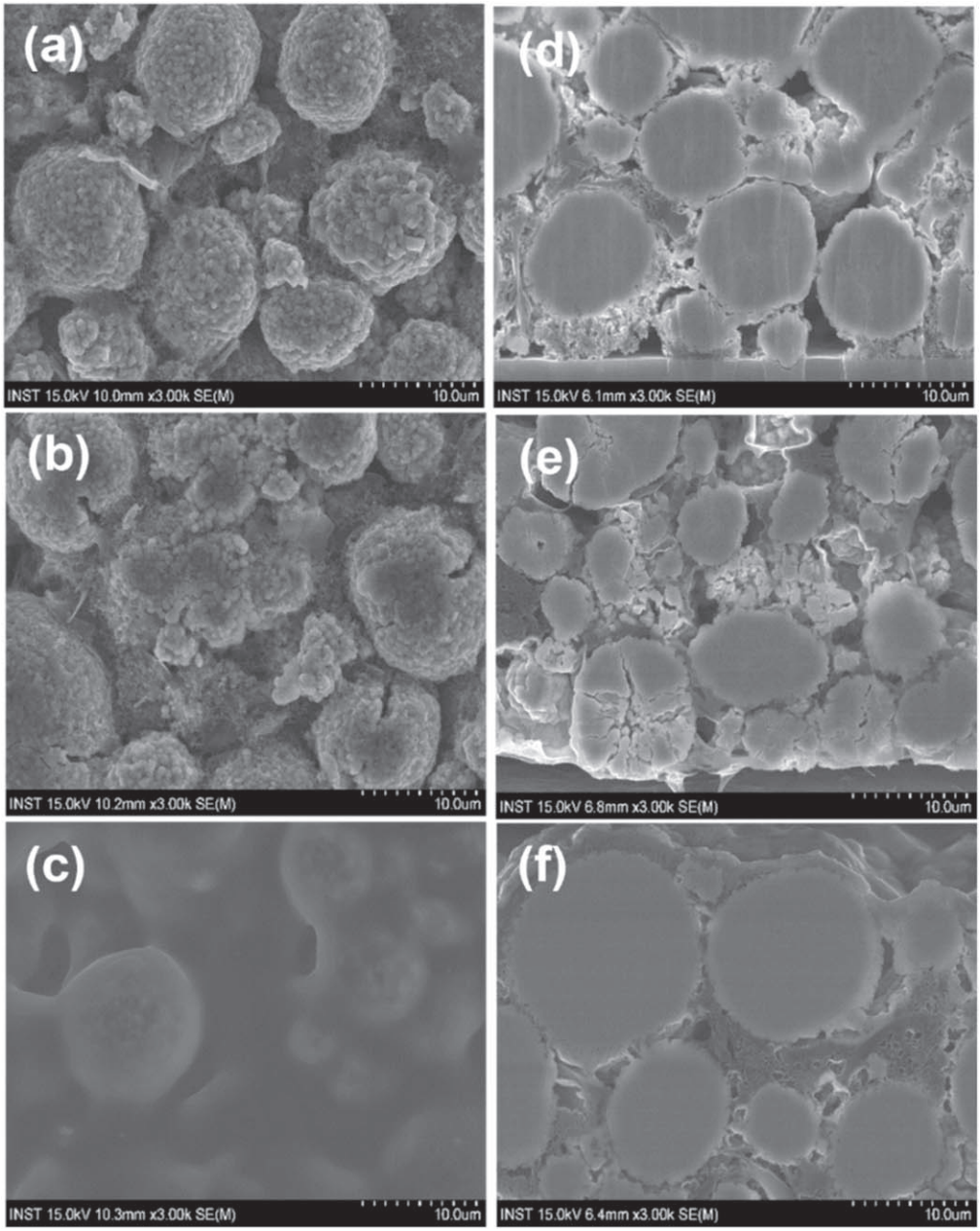

Figure 5. Surface SEM images of (a) pristine cathode and cathodes after 200 cycles in (b) liquid electrolyte and (c) quasi-solid-state electrolyte. Cross-sectional SEM images of (d) pristine cathode and cathodes after 200 cycles in (e) liquid electrolyte and (f) quasi-solid-state electrolyte.

The thermal stability of electrodes plays an important role in battery safety. In particular, the thermal stability of the electrodes containing electrolyte at fully charged state (lithiated anode and delithiated cathode) has been used as an index in predicting the battery safety.[38,39] To investigate the effect of electrolyte on the thermal stability of charged electrodes, the cell was cycled twice within the cut-off voltage of 3.0 to 4.2 V and then recharged to 4.2 V. We then disassembled the cell in an argon-filled glove box and collected the electrolyte-containing electrodes (anode and cathode) for DSC measurements. Figure 7a shows DSC thermograms of the charged cathodes with different electrolytes. The $Li_{1-x}Ni_{0.6}Co_{0.2}Mn_{0.2}O_2$ cathode containing liquid electrolyte exhibited two sharp exothermic peaks at 134.0 and 264.1 °C with heat flow of 41.2 and 482.9 J g^{-1}, respectively. The first exothermic peak at lower temperature is related to the thermal decomposition of the cathode electrolyte interphase (CEI) layer.[40] The second exothermic peak at higher temperature can be attributed to the oxygen generation by the structural deterioration of the delithiated cathode and the reaction with liquid electrolyte.[41,42] In contrast, the exothermic peak of the charged $Li_{1-x}Ni_{0.6}Co_{0.2}Mn_{0.2}O_2$ electrode with QSE was considerably decreased and broaden, showing an exothermic heat of 75.4 J g^{-1}. For anode with liquid electrolyte (Fig. 7b), there are one endothermic peak and two exothermic peaks. A small endothermic peak around 70 °C corresponds to the melting of EC-$LiPF_6$ crystalline complex.[39,43] The two exothermic peaks at 124.3 and 272.1 °C are attributed to the breakdown of SEI layer and exothermic

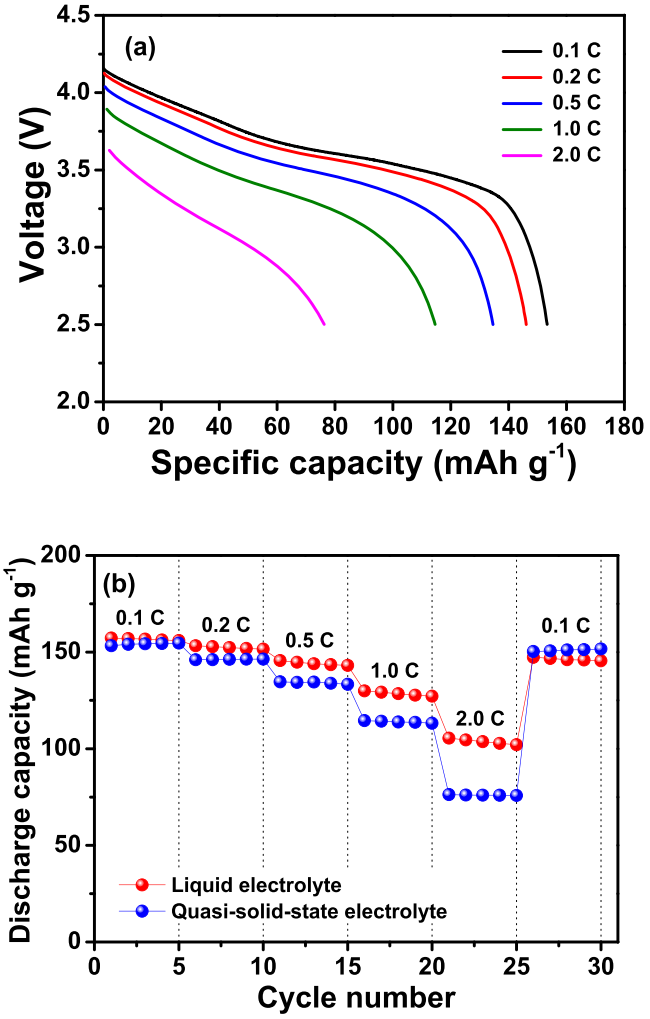

Figure 6. (a) Discharge curves of the lithium-ion cells employing QSE-S5 at different C rates and 25 °C. (b) Discharge capacities of the lithium-ion cells assembled with different electrolytes, which were obtained during every five cycles at different C rates.

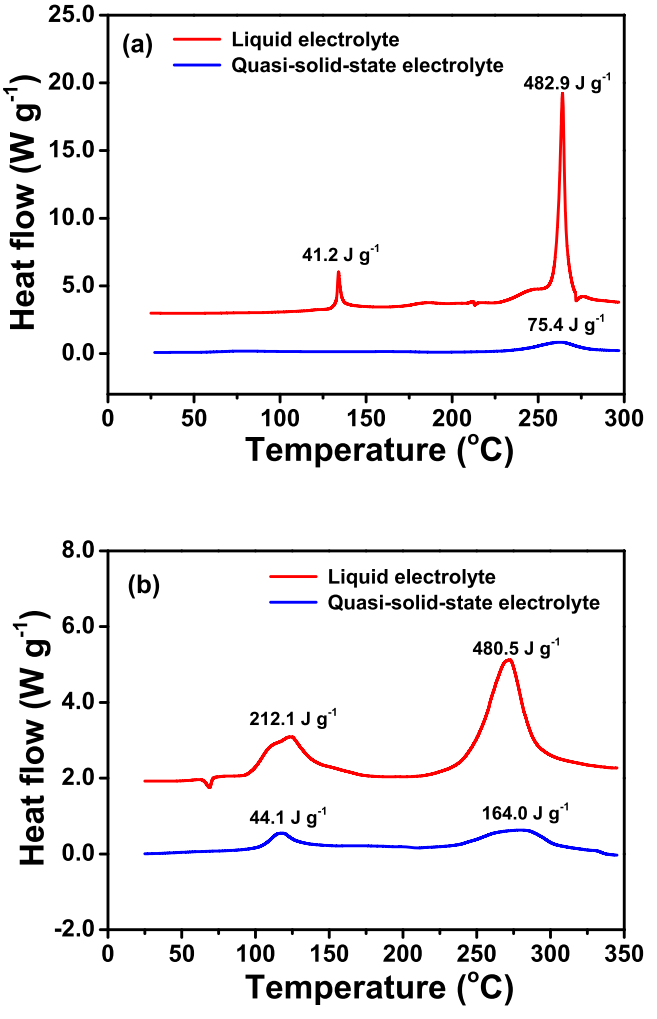

Figure 7. DSC thermograms of (a) delithiated $Li_{1-x}Ni_{0.6}Co_{0.2}Mn_{0.2}O_2$ cathodes and (b) lithiated Li_xC anodes cycled with liquid electrolyte and quasi-solid-state electrolyte (QSE-S5).

reactions between the lithiated graphite (Li_xC) and liquid electrolyte, respectively.[44,45] Like the cathode materials, the charged anode with QSE exhibited less exothermic heat than the anode with liquid electrolyte. These results indicate that the charged electrode materials ($Li_{1-x}Ni_{0.6}Co_{0.2}Mn_{0.2}O_2$ and Li_xC) are less reactive with QSE, and that structural stability of electrodes can be enhanced by replacing liquid electrolyte with QSE. Such an improved thermal stability of the electrode materials can lead the enhancement of the safety of the QSE-based battery.

Conclusions

We prepared a three-dimensional quasi-solid-state electrolyte by a click reaction with perfluoroether diacrylate and pentaerylythritol tetrakis(3-mercaptoptopionate) as the cross-linking agents. The optimized quasi-solid-state electrolyte had a high ionic conductivity of 2.1×10^{-3} S cm^{-1} at 25 °C and exhibited higher oxidative stability than liquid electrolyte. By employing quasi-solid state electrolyte, the lithium-ion cell exhibited good cycling stability and significantly enhanced thermal stability compared to the cell with liquid electrolyte. Our results demonstrate that the quasi-solid state electrolyte in this work can be a promising electrolyte for the lithium-ion battery requiring enhanced safety and stable cycleability.

Acknowledgments

This work was supported by LG Energy Solution, the National Research Foundation of Korea funded by the Korean government (2021R1A2C2011050) and the Technology Innovation Program (20012330) funded by the Ministry of Trade, Industry and Energy (MOTIE, Korea).

ORCID

Dong-Won Kim https://orcid.org/0000-0002-1735-0272

References

1. J.-M. Tarascon and M. Armand, "Issues and challenges facing rechargeable lithium batteries." *Nature*, **414**, 359 (2001).
2. M. Armand and J.-M. Tarascon, "Building better batteries." *Nature*, **451**, 652 (2008).
3. V. Etacheri, R. Marom, R. Elazari, G. Salitra, and D. Aurbach, "Challenges in the development of advanced Li-ion batteries: a review." *Energy Environ. Sci.*, **4**, 3243 (2011).
4. J. B. Goodenough and K. S. Park, "The Li-ion rechargeable battery: a perspective." *J. Am. Chem. Soc.*, **135**, 1167 (2013).
5. B. Dunn, H. Kamath, and J.-M. Tarascon, "Electrical energy storage for the grid: a battery of choices." *Science*, **334**, 928 (2011).
6. R. Van Noorden, "The rechargeable revolution: a better battery." *Nature*, **507**, 26 (2014).
7. D. Larcher and J.-M. Tarascon, "Towards greener and more sustainable batteries for electrical energy storage." *Nat. Chem.*, **7**, 19 (2015).

8. K. Deng, Q. Zeng, D. Wang, Z. Liu, G. Wang, Z. Qiu, Y. Zhang, M. Xiao, and Y. Meng, "Nonflammable organic electrolytes for high-safety lithium-ion batteries." *Energy Storage Mater.*, **32**, 425 (2020).
9. Q. Wang, L. Jiang, Y. Yu, and J. Sun, "Progress of enhancing the safety of lithium ion battery from the electrolyte aspect." *Nano Energy*, **55**, 93 (2019).
10. Y. Meesala, A. Jena, H. Chang, and R.-S. Liu, "Recent advancements in Li-Ion conductors for all-solid-state Li-ion batteries." *ACS Energy Lett.*, **2**, 2734 (2017).
11. F. Zheng, M. Kotobuki, S. Song, M. O. Lai, and L. Lu, "Review on solid electrolytes for all-solid-state lithium-ion batteries." *J. Power Sources*, **389**, 198 (2018).
12. Y. Zheng, Y. Yao, J. Ou, M. Li, D. Luo, H. Dou, Z. Li, K. Amine, A. Yu, and Z. Chen, "A review of composite solid-state electrolytes for lithium batteries: fundamentals, key materials and advanced structures." *Chem. Soc. Rev.*, **49**, 8790 (2020).
13. N. Boaretto, I. Garbayo, S. Valiyaveettil-Sobhan Raj, A. Quintela, C. Li, M. Casas-Cabanas, and F. Aguesse, "Lithium solid-state batteries: state-of-the-art and challenges for materials, interfaces and processing." *J. Power Sources*, **502**, 229919 (2021).
14. C. Wang, J. Liang, Y. Zhao, M. Zheng, X. Li, and X. Sun, "All-solid-state lithium batteries enabled by sulfide electrolytes: from fundamental research to practical engineering design." *Energy Environ. Sci.*, **14**, 2577 (2021).
15. M. Balaish, J. C. Gonzalez-Rosillo, K. J. Kim, Y. Zhu, Z. D. Hood, and J. L. M. Rupp, "Processing thin but robust electrolytes for solid-state batteries." *Nat. Energy*, **6**, 227 (2021).
16. H. Wang, L. Sheng, G. Yasin, L. Wang, H. Xu, and X. He, "Reviewing the current status and development of polymer electrolytes for solid-state lithium batteries." *Energy Storage Mater.*, **33**, 188 (2020).
17. W.-P. Chen et al., "Bridging interparticle Li^+ conduction in a soft ceramic oxide electrolyte." *J. Am. Chem. Soc.*, **143**, 5717 (2021).
18. H. Duan et al., "Building an air stable and lithium deposition regulable garnet interface from moderate-temperature conversion chemistry." *Angew. Chem. Int. Ed.*, **59**, 12069 (2020).
19. X. Judez, A. Santiago, M. Armand, H. Zhang, and C. Li, "Quasi-solid-state electrolytes for lithium sulfur batteries: advances and perspectives." *J. Power Sources*, **438**, 22698 (2019).
20. H. Son, H.-S. Woo, M.-S. Park, J. Y. Min, and D.-W. Kim, "Polyurethane-based elastomeric polymer electrolyte for lithium metal polymer cells with enhanced thermal safety." *J. Electrochem. Soc.*, **167**, 080525 (2020).
21. X. Judez, M. Martinez-Ibanez, A. Santiago, M. Armand, H. Zhang, and C. Li, "Quasi-solid-state electrolytes for lithium sulfur batteries: advanced and perspectives." *J. Power Sources*, **438**, 226985 (2019).
22. Z. Li, X.-Y. Zhou, and X. Guo, "High-performance lithium metal batteries with ultraconformal interfacialcontacts of quasi-solid electrolyte to electrodes." *Energy Storage Mater.*, **29**, 149 (2020).
23. S. Park, B. Jeong, D.-A. Lim, C. H. Lee, K. H. Ahn, J. H. Lee, and D.-W. Kim, "Quasi-solid-state electrolye synthesized using a thiol-ene click chemistry for rechargeable lithium metal batteries with enhanced safety." *ACS Appl. Mater. Interfaces*, **12**, 19553 (2020).
24. K. Nishio, Y. Gambe, J. Kawaji, A. Unemoto, T. Okumura, and I. Honma, "High rate capability of all-solid-state lithium batteries using quasi-solid-state electrolytes containing ionic liquids." *J. Electrochem. Soc.*, **167**, 040511 (2020).
25. C. E. Hoyle, T. Y. Lee, and T. Roper, "Thiol–enes: chemistry of the past with promise for the future." *J. Polym. Sci., Part A: Polym. Chem.*, **42**, 5301 (2004).
26. C. E. Hoyle and C. N. Bowman, "Thiol–ene click chemistry." *Angew. Chem. Int. Ed.*, **49**, 1540 (2010).
27. D. P. Nair, M. Podgorski, S. Chatani, T. Gong, W. Xi, C. R. Fenoli, and C. N. Bowman, "The thiol-michael addition click reaction: a powerful and widely used tool in materials chemistry." *Chem. Mater.*, **26**, 724 (2014).
28. J. Zhang, S. Wang, D. Han, M. Xiao, L. Sun, and Y. Meng, "Lihtium (4-styrenesulfonyl) (trifluoromethanesulfonyl) imide based single-ion polymer electrolyte with superior battery performance." *Energy Storage Mater.*, **24**, 579 (2020).
29. Z. Yu et al., "Molecular design for electrolyte solvents enabling energy-dense and long-cycling lithium metal batteries." *Nat. Energy*, **5**, 526 (2020).
30. P. Jaumaux, Q. Liu, D. Zhou, X. Xu, T. Wang, Y. Wang, F. Kang, B. Li, and G. Wang, "Deep-eutectic-solvent-based self-healing polymer electrolyte for safe and long-life lithium-metal batteries." *Angew. Chem. Int. Ed.*, **59**, 9134 (2020).
31. Z. Lv, Q. Zhou, S. Zhang, S. Dong, Q. Wang, L. Huang, K. Chen, and G. Cui, "Cyano-reinforced in situ polymer electrolyte enabling long-life cycling for high-voltage lithium metal batteries." *Energy Storage Mater.*, **37**, 215 (2021).
32. P. Keil, S. F. Schuster, J. Wilhelm, J. Travi, A. Hauser, R. C. Karl, and A. Jossen, "Calendar aging of lihtium-ion batteries." *J. Electrochem. Soc.*, **163**, A1872 (2016).
33. Y. L. Ruan, X. Y. Song, Y. B. Fu, C. Y. Song, and V. Battaglia, "Structural evolution and capacity degradation mechanism of $LiNi_{0.6}Mn_{0.2}Co_{0.2}O_2$ cathode materials." *J. Power Sources*, **400**, 539 (2018).
34. S. Hashigami, Y. Kato, K. Yoshimi, H. Yoshida, T. Inagaki, M. Hashinokuchi, T. Doi, and M. Inaba, "Influence of lithium silicate coating on retarding crack formation in $LiNi_{0.5}Co_{0.2}Mn_{0.3}O_2$ cathode particles." *Electrochim. Acta*, **291**, 304 (2018).
35. J. H. Kim, H. H. Ryu, S. J. Kim, C. S. Yoon, and Y. K. Sun, "Degradation mechanism of highly Ni-rich $Li[Ni_xCo_yMn_{1-x-y}]O_2$ cathodes with x>0.9." *ACS Appl. Mater. Interfaces*, **11**, 30936 (2019).
36. H. Ma, D. Hwang, Y. J. Ahn, M. Y. Lee, S. Kim, Y. Lee, S. M. Lee, S. K. Kwak, and N. S. Choi, "In situ interfacial tuning to obtain high-performance nickel-rich cathodes in lihtium metal batteries." *ACS Appl. Mater. Interfaces*, **11**, 29365 (2020).
37. L. Bodenes, R. Naturel, H. Martinez, R. Dedryvere, M. Menetrier, L. Croguennec, J. P. Peres, C. Tessier, and F. Fischer, "Lithium secondary batteries working at very high temperature: capacity fade and understanding of aging mechanisms." *J. Power Sources*, **236**, 265 (2013).
38. L. Zhang, J. Liu, P. Fan, L. Du, Y. Ma, B. Qu, G. Yin, Q. Fu, F. Yang, and C. Zhang, "Unraveling the effect of short-term high-temperature storage on the performance and thermal stability of $LiNi_{0.5}Co_{0.2}Mn_{0.3}O_2$/graphite battery." *J. Power Sources*, **459**, 227842 (2020).
39. J. Hou, M. Yang, D. Wang, and J. Zhang, "Fundamentals and challenges of lithium ion batteries at temperatures between −40 and 60 °C." *Adv. Energy Mater.*, **10**, 1904152 (2020).
40. H. Maleki, G. Deng, A. Anami, and J. Howard, "Thermal stability studies of Li-Ion cells and components." *J. Electrochem. Soc.*, **146**, 3224 (1999).
41. P. Roder, B. Stiaszny, J. C. Ziegler, N. Baba, P. Lagaly, and H. D. Wiemhofer, "The impact of calendar aging on the thermal stability of a $LiMn_2O_4$-$Li(Ni_{1/3}Mn_{1/3}Co_{1/3})O_2$ /graphite lithium-ion cell." *J. Power Sources*, **268**, 315 (2014).
42. H. Yang et al., "Simultaneously dual modification of Ni-rich layered oxide cathode for high-energy lithium-ion batteries." *Adv. Funct. Mater.*, **29**, 1808825 (2019).
43. H. Maleki, G. Deng, A. Anani, and J. Howard, "Thermal stability Studies of Li-Ion cells and components." *J. Electrochem. Soc.*, **146**, 3224 (1999).
44. Y.-S. Park and S.-M. Lee, "Effects of lithium phosphorous oxynitride film coating on electrochemical performance and thermal stability of graphite anodes." *J. Phys. Chem. Solid.*, **72**, 842 (2011).
45. O. Haik, S. Ganin, G. Gershinsky, E. Zinigrad, B. Markovsky, D. Aurbach, and I. Halalay, "On the thermal behavior of lithium intercalated graphites." *J. Electrochem. Soc.*, **158**, A913 (2011).